Journal of Hazardous Materials 198 (2011) 282–290

Contents lists available at SciVerse ScienceDirect

Journal of Hazardous Materials

journal homepage: www.elsevier.com/locate/jhazmat

Removal of methylene blue from aqueous solution with magnetite loaded multi-wall carbon nanotube: Kinetic, isotherm and mechanism analysis

Lunhong Ai[a,b,*], Chunying Zhang[b], Fang Liao[a,b], Yao Wang[a,b], Ming Li[b], Lanying Meng[b], Jing Jiang[a,b,*]

[a] Chemical Synthesis and Pollution Control Key Laboratory of Sichuan Province, China West Normal University, Shida Road 1#, Nanchong 637002, PR China
[b] College of Chemistry and Chemical Engineering, China West Normal University, Shida Road 1#, Nanchong 637002, PR China

ARTICLE INFO

Article history:
Received 19 May 2011
Received in revised form 1 October 2011
Accepted 13 October 2011
Available online 18 October 2011

Keywords:
Magnetite
Multi-walled carbon nanotubes
Adsorption
Methylene blue

ABSTRACT

In this study, we have demonstrated the efficient removal of cationic dye, methylene blue (MB), from aqueous solution with the one-pot solvothermal synthesized magnetite-loaded multi-walled carbon nanotubes (M-MWCNTs). The as-prepared M-MWCNTs were characterized by X-ray diffraction (XRD), scanning electron microscopy (SEM), and Fourier transform infrared (FTIR) spectroscopy. The effects of contact time, initial dye concentration, and solution pH on the adsorption of MB onto M-MWCNTs were systematically studied. It was shown that the MB adsorption was pH-dependent. Adsorption kinetics was best described by the pseudo-second-order model. Equilibrium data were well fitted to the Langmuir isotherm model, yielding maximum monolayer adsorption capacity of 48.06 mg g^{-1}. FTIR analysis suggested that the adsorption mechanism was possibly attributed to the electrostatic attraction and $\pi-\pi$ stacking interactions between MWCNTs and MB.

1. Introduction

Dyes are one of the most hazardous materials in industrial effluents which can cause severe health problems in human beings, since they exhibit high biotoxicity and potential mutagenic and carcinogenic effects [1,2]. Therefore, the removal of dye from colored effluents has attracted increasing attention. Several technologies including biological treatment, adsorption, coagulation/flocculation, chemical oxidation, membrane separation and ion exchange have been developed [3–8]. Among these methods, adsorption has been considered to be simple, highly efficient, and ease of operation. A wide range of materials have been reported for dye removal, including activated carbon, zeolite, clay, polymer, etc. [9–12]. In view of pollutant control at present, it is still indispensible for the development of new adsorbent materials with high adsorption capacities and removal efficiencies.

Recently, carbon nanotubes (CNTs) have attracted great interest as a new type of adsorbent for removing environmental pollutants (e.g. small molecules, heavy metal ions, radionuclides, and organic chemicals) [13], due to their remarkable features of the large specific surface area, hollow and layered structures. However, recovery of this kind of adsorbent usually needs the complicated and time-consuming filtration and/or centrifugation, thus limiting the reusability and increasing the regeneration cost. In this regard, many researchers have focused on combining CNTs and magnetic oxides to create a promising novel adsorbent that possesses adsorptive and magnetic dual functionalities [14–16], which opens new opportunities for the achievement of desirable adsorption capacity and effective magnetic separation. For example, Luan et al. synthesized CNTs/iron oxide composites by a chemical coprecipitation method with a high performance for the removal of Pb(II) and Cu(II) from water [17]. Gong et al. demonstrated chemical coprecipitation derived MWCNTs/iron oxide composites can efficiently remove cationic dye from aqueous solution [18]. Mishra and Ramaprabhu also employed chemical coprecipitation method to synthesize MWCNTs/magnetite composites for the removal of high concentration of arsenic and desalination of seawater [19]. However, to the best of knowledge, there is little report on the adsorption behavior of the solvothermally synthesized MWCNTs/magnetite composites.

In the present work, we have demonstrated a one-pot solvothermal route to prepare the magnetite (Fe_3O_4)-loaded multi-walled carbon nanotubes (M-MWCNTs) as an efficient adsorbent for the removal of cationic dye, methylene blue (MB), from aqueous solution. The effect of various parameters such as contact time, solution pH and initial dye concentration on the adsorption of MB onto M-MWCNTs was systematically studied. Adsorption isotherm, kinetic and mechanism were also evaluated. Furthermore, the resulting M-MWCNTs presented high magnetic sensitivity under an external magnetic field, providing an easy and efficient way for the separation of adsorbent from aqueous solution.

* Corresponding authors at: Chemical Synthesis and Pollution Control Key Laboratory of Sichuan Province, China West Normal University, Shida Road 1#, Nanchong 637002, PR China. Tel.: +86 817 2568081; fax: +86 817 2224217.
E-mail address: ah_aihong@163.com (L. Ai).

0304-3894/$ – see front matter © 2011 Elsevier B.V. All rights reserved.
doi:10.1016/j.jhazmat.2011.10.041

2. Experimental

2.1. Materials

$FeCl_3{\cdot}6H_2O$, sodium acetate (NaAc), ethylene glycol (EG), methylene blue (MB) were purchased from Sinopharm Chemical Reagent Co., Ltd. (Shanghai, China) and used without further purification. All chemicals used in this study were of commercially available analytical grade. Multi-walled carbon nanotubes were purchased from Shenzhen Nanotech Port Ltd. Co. (Shenzhen, China). The detailed parameters supplied by the manufacturer are as follows: length: 5–15 μm; diameter: 20–40 nm; purity: ≥95%; ash: ≤0.2 wt%; amorphous carbon: <3%. MWCNTs were purified via being dispersed in concentrated nitric acid at 60 °C with constant stirring for 12 h, followed by filtering and washing with distilled water several times until the pH value reached neutral, and then filtered and dried in vacuum at 60 °C for further use.

2.2. Preparation of magnetite loaded MWCNTs (M-MWCNTs)

In a typical synthesis, 0.8 g purified MWCNTs were dispersed in 70 mL EG solution by ultrasonication for 30 min. Afterward, 1.6 g $FeCl_3{\cdot}6H_2O$ and 3.2 g NaAc were then added to EG solution at ambient temperature. After stirring for about 30 min, the solution was transferred into a 100 mL Teflon-lined stainless-steel autoclave and kept at 200 °C for 6 h followed by cooling to ambient temperature naturally. The black precipitate was centrifuged, washed with ethanol several times, and finally dried at 60 °C in a vacuum oven.

2.3. Characterization

The powder X-ray diffraction (XRD) measurements were recorded on a Rigaku Dmax/Ultima IV diffractometer with monochromatized Cu Kα radiation (λ = 0.15418 nm). The morphology was observed with a JSM-6510 scanning electron microscope (SEM). The Fourier transform infrared (FTIR) spectroscopy was measured on Nicolet 6700 FTIR Spectrometric Analyzer using KBr pellets. A pHS-3C digital pH meter (Rex Instruments Factory, Shanghai, China) was employed for the pH measurements. The point of zero charge (pH_{PZC}) of the adsorbent was determined by the solid addition method. To a series of 100 mL conical flasks, 45 mL of 0.1 mol L^{-1} NaCl solution was transferred. The initial pH values (pH_i) of the solution were adjusted from 1.0 to 11.0 by adding either 0.1 mol L^{-1} HCl or 0.1 mol L^{-1} NaOH. The total volume of the solution in each flask was made exactly to 50 mL by adding the NaCl solution. Then, 0.1 g of M-MWCNTs was added to each flask and the mixtures were agitated at 150 rpm. After 48 h, the final pH values (pH_f) of the solutions were measured. The difference between the initial and final pH values ($\Delta pH = pH_i - pH_f$) was plotted against the pH_i. The point of intersection of the resulting curve with abscissa, at which $\Delta pH = 0$, gave the pH_{PZC}.

2.4. Adsorption experiments

Batch adsorption experiments were carried out in a thermostated shaker with a shaking speed of 150 rpm using 100 mL Erlenmeyer flasks and conducted in duplicate. To study the adsorption isotherms, 0.02 g of M-MWCNTs were added into 50 mL of MB solutions of different initial concentrations (10–30 mg L^{-1}) at natural pH in flask, and agitated in a temperature-controlled shaker at 25 ± 1 °C for 120 min. The concentration of MB left in the supernatant solution was determined by using a UV–vis spectrophotometer (Shimadzu, UV-2550). The amount of MB adsorbed per unit mass of M-MWCNTs was calculated according to Eq. (1):

$$q = \frac{(C_0 - C_e)V}{m} \quad (1)$$

where C_0 and C_e are the initial and equilibrium concentrations of MB (mg L^{-1}), m is the mass of M-MWCNTs (g), and V is the volume of solution (L).

Batch kinetic experiments were carried out by mixing 0.02 g of M-MWCNTs to 50 mL of MB solution with a known initial concentration (10, 20 and 30 mg L^{-1}) at natural pH and agitated in a temperature-controlled shaker at 25 ± 1 °C for different time interval (5–280 min). The concentration of MB left in the supernatant solution was analyzed as above.

The effect of pH was performed by dispersion of 0.02 g of M-MWCNTs in 50 mL of MB solution of 20 mg L^{-1}. The initial pH of MB solution was adjusted to values in the range of 2.0–10.0 by the addition of 0.1 mol L^{-1} HCl or 0.1 mol L^{-1} NaOH solutions. The suspensions were agitated in a temperature-controlled shaker at 25 ± 1 °C for 120 min. The concentration of MB left in the supernatant solution was analyzed as above.

2.5. Leaching test

To evaluate the stability of M-MWCNTs, the leaching of iron ions from M-MWCNTs at different pH levels was investigated. 0.02 g of M-MWCNTs was dispersed in 50 mL aqueous solution with pH ranging from 2.0 to 10.0 and agitated in a temperature-controlled shaker at 25 ± 1 °C for 280 min. The leached Fe concentration in the supernatant was determined by a WFX-120 atomic absorption spectroscopy (AAS, Rayleigh Analytical Instrument Corp., China).

3. Results and discussion

3.1. Characterization of the adsorbent

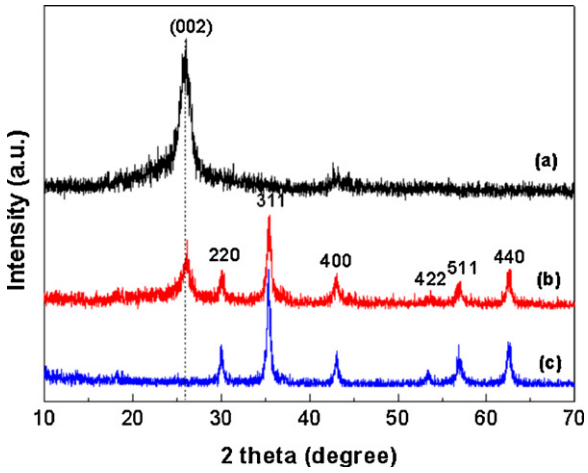

Fig. 1. XRD patterns of MWCNTs (a), M-MWCNTs (b) and Fe_3O_4 (c).

Fig. 1 shows the X-ray diffraction (XRD) patterns of MWCNTs, Fe_3O_4 and M-MWCNTs. As for MWCNTs (Fig. 1(a)), the strong diffraction peak at $2\theta = 25.8°$ can be indexed as the (0 0 2) reflection of the hexagonal graphite structure. After loading of Fe_3O_4 (Fig. 1(b)), besides the diffraction peak of MWCNTs, the new peaks at 2θ values of 18.2° (1 1 1), 30.0° (2 2 0), 35.3° (3 1 1), 42.9° (4 0 0), 53.4° (4 2 2), 56.9° (5 1 1), and 62.5° (4 4 0) are observed, which are consistent with the standard XRD data for the cubic phase Fe_3O_4 (JCPDS no. 89-4319) with a face-centered cubic (fcc) structure, indicating the coexistence of Fe_3O_4 and MWCNTs in the M-MWCNTs.

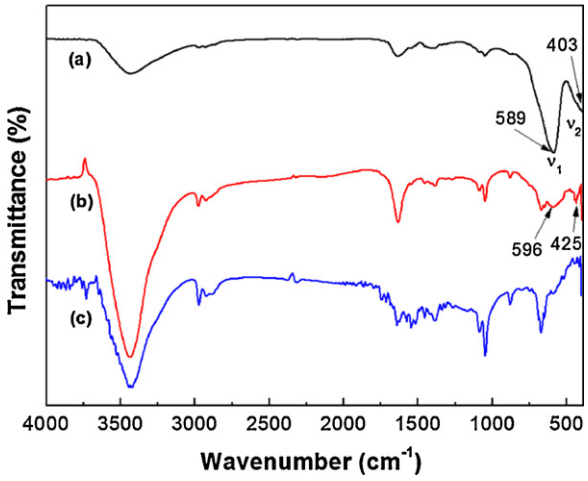

Fig. 2. FTIR spectra of Fe_3O_4 (a), M-MWCNTs (b) and MWCNTs (c).

Fig. 2 shows the FTIR spectra of Fe_3O_4, MWCNTs, and M-MWCNTs. In spinel ferrites, the metal ions are situated in two different sublattices, designated tetrahedral and octahedral according to the geometrical configuration of the oxygen nearest neighbors. Waldron [20] has studied the vibrational spectra of ferrites and attributed a high-frequency band ν_1 to the intrinsic vibration of the tetrahedral sites and a low-frequency band ν_2 to the octahedral site. In this case, the observed prominent peaks at 589 and 403 cm^{-1} in FTIR spectrum of Fe_3O_4 (Fig. 2(a)) are ascribed to the intrinsic vibrations of the tetrahedral and octahedral sites, respectively, corresponding to the ν(Fe–O) modes. As shown in Fig. 2(b), MWCNTs exhibits the characteristic absorption peaks at 3430 cm^{-1} (the O–H stretching mode), 1635 cm^{-1} (the C=O stretching mode), 1452 cm^{-1} (the C=C stretching mode), 1385 cm^{-1} (the O–H bending modes), 1046 and 1092 cm^{-1} (the C–O stretching modes) [21–23], which suggests the surface of MWCNTs possesses a certain amount of oxygen-containing functional groups, thus providing some reactive and anchoring sites for nucleation and growth of magnetic particles [19,24,25]. It should be noted that the absorption peaks of M-MWCNTs (Fig. 2(c)) are almost identical to that of MWCNTs, but characteristic peaks of Fe_3O_4 in M-MWCNTs is shifted to higher wavenumbers (596 and 425 cm^{-1}), indicating the appearance of interaction between Fe_3O_4 and MWCNTs [26,27].

Fig. 3(a) shows a typical SEM image of MWCNTs. They are randomly aligned with a diameter of approximately 20–40 nm and a length of several micrometers. A typical SEM image of the Fe_3O_4 displayed in Fig. 3(b) shows that the product is composed of a large quantity of nearly uniform monodispersed spheres. These spheres with smooth surfaces have a diameter of about 200 nm. After the combination with MWCNTs (Fig. 3(c)), the Fe_3O_4 spheres are uniformly loaded on the network structure of MWCNTs with a high density.

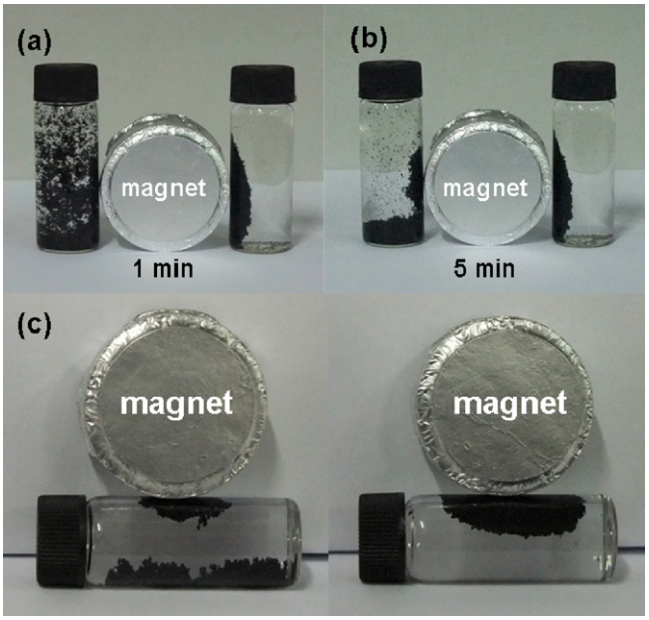

Fig. 4. Magnetic response of the M-MWCNTs and the physical mixtures of MWCNTs and Fe_3O_4 to an external magnetic field in different directions, left: the physical mixtures of MWCNTs and Fe_3O_4, right: M-MWCNTs.

Fig. 4 shows the magnetic response behavior of the M-MWCNTs and the physical mixture of MWCNTs and Fe_3O_4 in water under an external magnetic field. The M-MWCNTs show a rapid response to an applied external magnetic field, which are attracted toward the magnet in a very short period, demonstrating its high magnetic sensitivity. In contrast, the two components in the physical mixture are easily separated by an applied external magnetic field, in which the magnetic component moves to the side of vial near magnet but the nonmagnetic component settles to the bottom of vial. Furthermore, the magnetic component exhibits a weak magnetic response behavior due to the resistance of the nonmagnetic component. Previously, Deng et al. [28] and Lin et al. [29] have demonstrated that the attachment of magnetic silica nanoparticles to carbon nanotubes would not occur by simply mixing the nanoparticles and CNTs. In the present study, the good magnetic response of the M-MWCNTs to external magnetic field could be ascribed to the formed interaction between MWCNTs and Fe_3O_4 nanoparticles [29,30], consistent with the results of FTIR analysis.

Fig. 5 shows a schematic illustration of the synthesis process of the magnetically separable M-MWCNTs. First, treating MWCNTs with nitric acid could introduce some carboxylic groups on the outside surface of MWCNTs, which would serve as reactive and anchoring sites for nucleation and growth of magnetic particles.

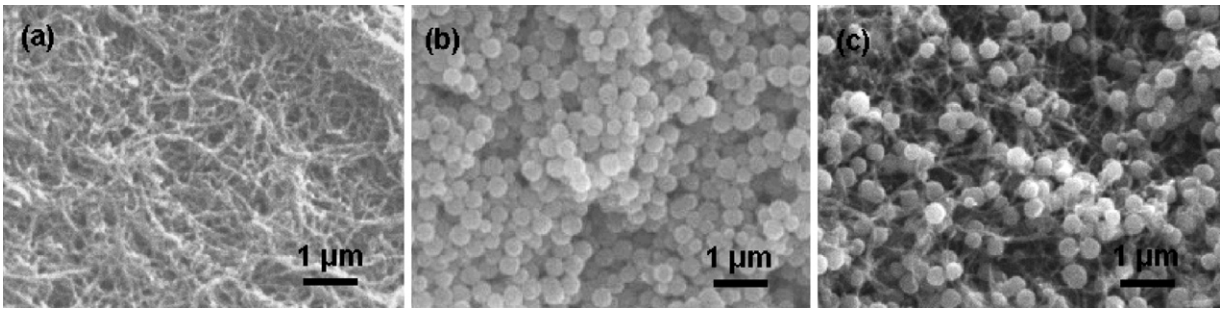

Fig. 3. SEM images of MWCNTs (a), Fe_3O_4 (b) and M-MWCNTs (c).

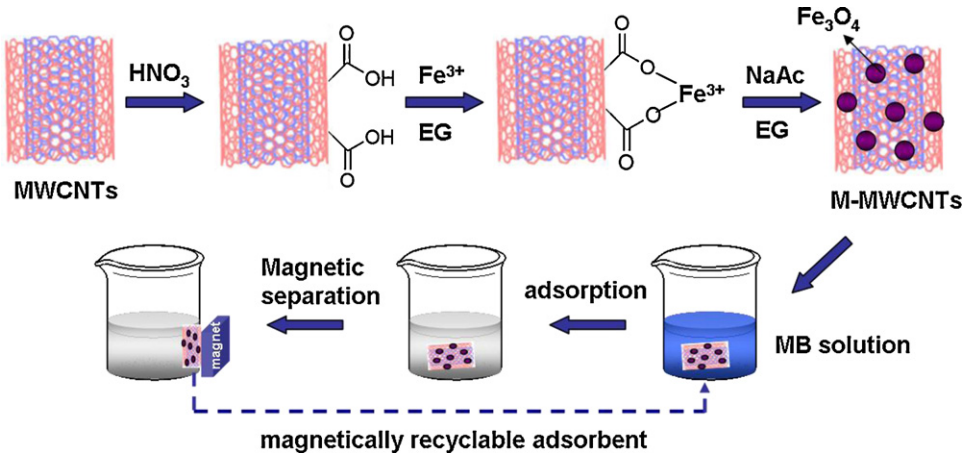

Fig. 5. Schematic illustration of the synthesis and application of the M-MWCNTs.

During the solvothermal treatment, the added Fe^{3+} ions were partial reduced into Fe^{2+} ions and further *in situ* converted to Fe_3O_4 and finally grew to form sphere-shaped structure on the network of MWCNTs. As for this multifunctional structure, MWCNTs can provide active adsorption sites for the efficient removal of dye pollutes in water. In turn, Fe_3O_4 attached on MWCNTs can introduce the magnetic function to gain a facile magnetic separation from water with the help of an external magnetic field.

3.2. Effect of pH

It is known that the solution pH can affect the surface charge of the adsorbent, the degree of ionization of the different pollutants, the dissociation of functional groups on the active sites of the adsorbent as well as the structure of the dye molecule. So the solution pH is an important parameter during the dye adsorption process. Fig. 6 shows the effect of initial pH on MB adsorption onto M-MWCNTs. The adsorption of MB onto M-MWCNTs is intimately dependent on solution pH. The adsorption capacity of MB increases with increasing solution pH from 2.0 to 7.0, and changes slightly when solution pH is above 7.0. The surface charge assessed by point of zero charge (pH_{PZC}) is defined as the point where the zeta potential is zero. When $pH < pH_{PZC}$, the surface charge is positive, and when $pH > pH_{PZC}$, the surface charge is negative. In this case, the pH_{PZC} of the M-MWCNTs determined by the solid addition method (Fig. 7) is about 6.5. When the solution pH is below pH_{PZC}, the M-MWCNTs acquire a positive surface charge. The competitive effects of H^+ ions and the electrostatic repulsion between the cationic dye molecules and the positively charged active adsorption sites on the M-MWCNTs would result in a decrease in the adsorption capacity of dye. In contrast, the surface of the M-MWCNTs may get negative charged at a solution pH higher than pH_{PZC}. Accordingly, the electrostatic attraction occurs between the negatively charged active adsorption sites and cationic dye molecule, which benefits for the adsorption of dye. Fig. 6 also demonstrates the solution pH values change during the adsorption process. At low initial pH ($pH_i < 7$), the final pH values (pH_f) are higher than pH_i values, due to an acid neutralization effect and proton adsorption of the surface of the M-MWCNTs [31,32]. The pH_f reaches 6.9–7.2 when the pH_i ranges from 7 to 10, indicating a buffering capacity caused by the adsorbent [33].

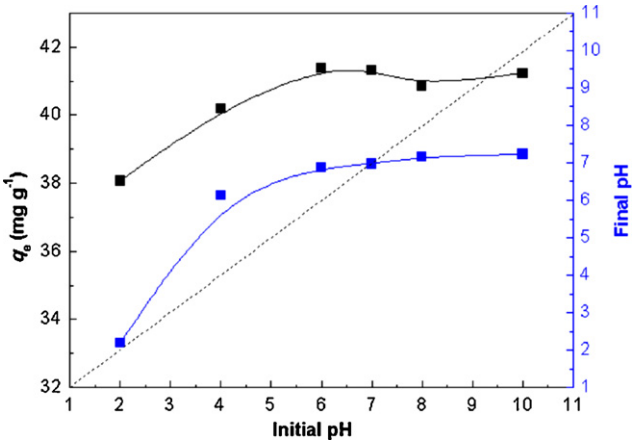

Fig. 6. Effect of solution pH on the adsorption of MB onto the M-MWCNTs.

3.3. Effect of contact time and initial MB concentration

Fig. 8 shows the effect of contact time on the adsorption capacity and percent removal of MB onto the M-MWCNTs at different initial concentrations. The adsorption capacity and percent removal of MB onto the M-MWCNTs drastically increase during the initial adsorption stage and then continue to increase at a relatively slow speed with contact time until a state of equilibrium is attained after 120 min. This phenomenon is attributed to the fact that a large number of vacant surface sites are available for adsorption at the initial stage, and after a lapse of time, the remaining vacant surface sites are difficult to be occupied due to

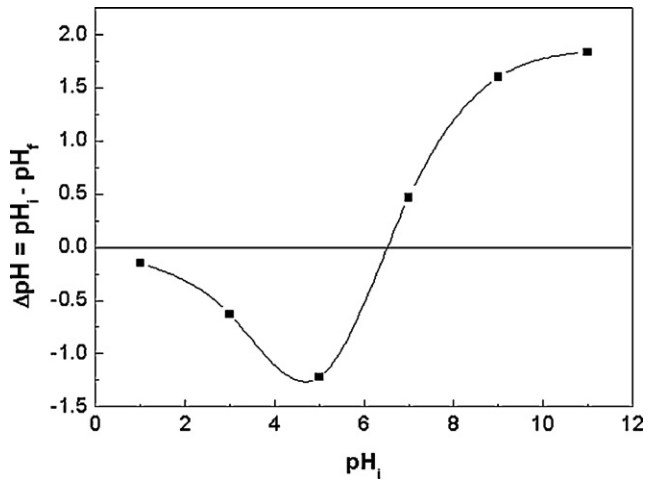

Fig. 7. Determination of the point of zero charge of the M-MWCNTs by the solid addition method.

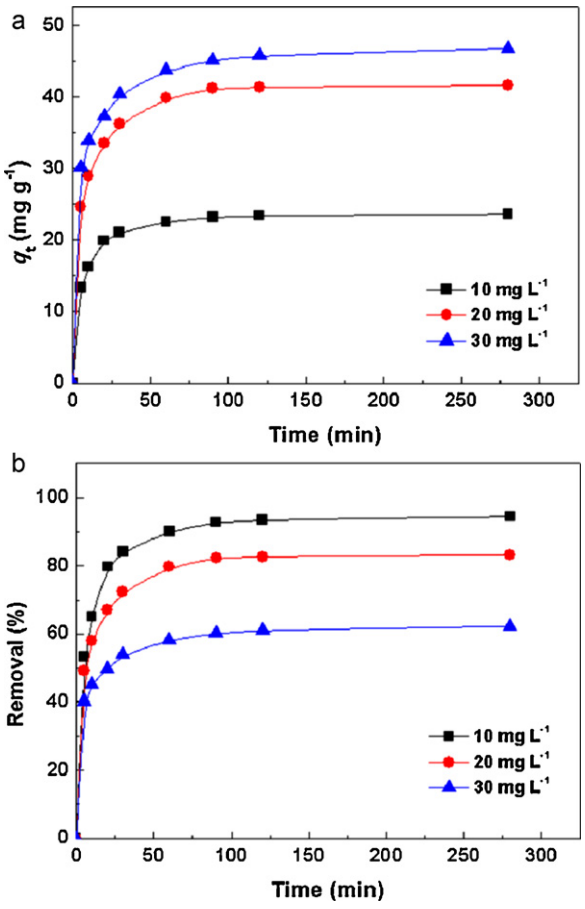

Fig. 8. The effect of contact time on the adsorption capacity (a) and percent removal (b) of MB onto the M-MWCNTs at different initial concentrations.

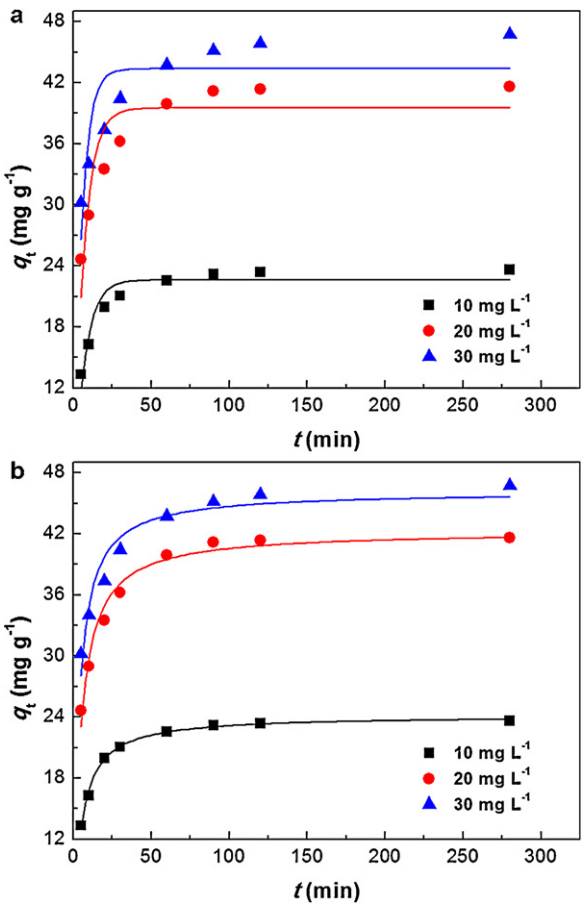

Fig. 9. Pseudo-first-order (a) and pseudo-second-order (b) kinetics for the adsorption of MB onto the M-MWCNTs.

repulsive forces between the solute molecules on the solid and bulk phases. Notably, the adsorption capacity of MB increases (Fig. 8(a)) but the percent removal of MB decreases with the increase in initial concentration (Fig. 8(b)), suggesting that the adsorption of MB onto M-MWCNTs is highly dependent on initial concentration. The initial dye concentrations provide an important driving force to overcome the mass transfer resistance of the dye between the aqueous phases and the solid phases, so increasing initial concentrations would enhance the adsorption capacity of dye. On the other hand, the dye adsorption process generally involves the first transport of dye molecules from bulk solution through liquid film to the exterior surface of adsorbent and then from the exterior surface to the pores of the adsorbent, which reflects the adsorption of dye onto the adsorbent is relevant to the initial concentration. In general, the total number of available adsorption sites is fixed for a given adsorbent dose. It is reasonable to particulate that the larger ratio of active adsorption sites of the adsorbent is available at lower initial concentration. Therefore, the percentage removal of dye is greater at lower initial concentration but smaller at higher initial concentration.

3.4. Adsorption kinetics

In order to further understand the characteristics of the adsorption process, the pseudo-first-order and pseudo-second-order kinetic models were applied to fit experimental data obtained from batch experiments. The pseudo-first-order and pseudo-second-order kinetic models are expressed in nonlinear form as follows [34,35]:

$$q_t = q_e - q_e e^{-k_1 t} \quad (2)$$

$$q_t = \frac{k_2 q_e^2 t}{1 + k_2 q_e t} \quad (3)$$

where q_e and q_t (mg g^{-1}) are the amounts of MB adsorbed at equilibrium and at time t (min), respectively. k_1 (min^{-1}) is the pseudo-first-order rate constant and k_2 (g mg^{-1} min^{-1}) is the pseudo-second-order rate constant. The kinetic parameters and the correlation coefficients (R^2) were determined by nonlinear regression (Fig. 9) and were given in Table 1. The calculated q_e values ($q_{e,cal}$) of both models are close to the experimental ones ($q_{e,exp}$). However, the R^2 values of the pseudo-second-order kinetic model

Table 1
Kinetic parameters for the adsorption of MB onto the M-MWCNTs.

C_0 (mg L^{-1})	$q_{e,exp}$ (mg g^{-1})	Pseudo-first-order			Pseudo-second-order		
		k_1 (min^{-1})	$q_{e,cal}$ (mg g^{-1})	R^2	k_2 (g mg^{-1} min^{-1})	$q_{e,cal}$ (mg g^{-1})	R^2
10	23.39	0.1434	22.61	0.8884	0.0096	24.14	0.9934
20	41.37	0.1506	39.50	0.7858	0.0057	42.23	0.9705
30	45.84	0.1905	43.36	0.6597	0.0067	46.13	0.9321

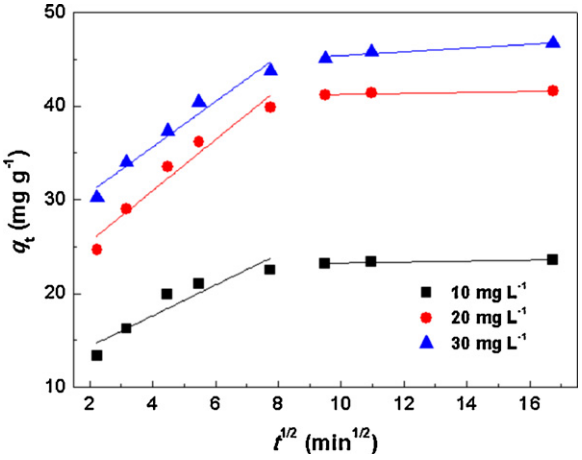

Fig. 10. Intraparticle diffusion plots for the adsorption of MB onto the M-MWCNTs.

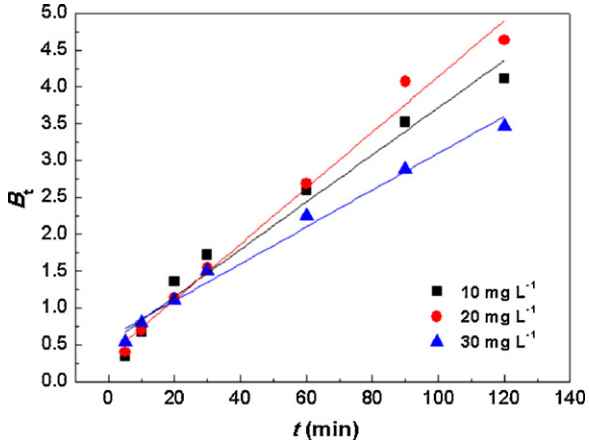

Fig. 11. Boyd plots for the adsorption of MB onto the M-MWCNTs.

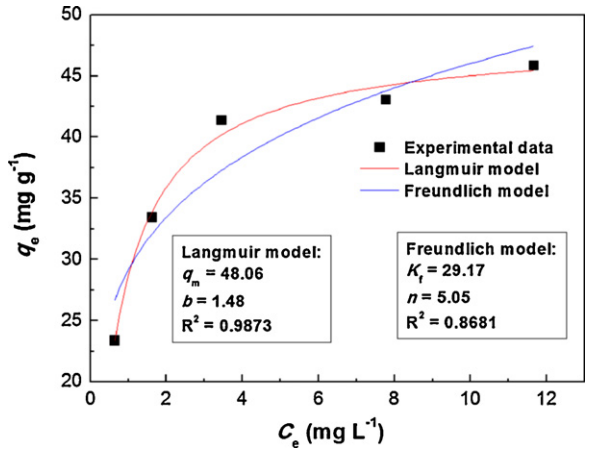

Fig. 12. Isotherms for the adsorption of MB onto the M-MWCNTs.

are much higher than those of pseudo-first-order kinetic model, implying that the kinetics of MB adsorption follows the pseudo-second-order kinetic model.

The Weber's intraparticle diffusion model was further employed to identify the steps involved during adsorption process, which is described as [36]:

$$q_t = k_i t^{1/2} + C \tag{4}$$

where k_i is the intraparticle diffusion rate constant (mg g^{-1} min$^{-1/2}$), C is a constant (mg g^{-1}). As shown in Fig. 10, plots present multilinearity, thus indicating that two or more steps take place. The initial region is a diffusion adsorption stage, attributing to the diffusion of dye through the solution to the external surface of adsorbent (external diffusion). The second region is a gradual adsorption stage, corresponding to intraparticle diffusion of dye molecules through the pores of adsorbent (intraparticle diffusion). Therefore, both film diffusion and intraparticle diffusion processes are simultaneously operating MB adsorption onto M-MWCNTs. The observed multilinearity also suggests that intraparticle diffusion is not the rate-limiting step. The values of k_i and C were calculated from the slope and intercept of plots of q_t versus $t^{1/2}$ (Fig. 10) and were summarized in Table 2.

To establish the actual rate-controlling step involved in the MB adsorption process, the adsorption kinetic data were further analyzed by Boyd kinetic model, which is expressed as [37]:

$$F = 1 - \frac{6}{\pi^2}\exp(-B_t) \tag{5}$$

where F is the fraction of solute adsorbed at different time t and B_t is a mathematical function of F and is given by

$$F = \frac{q_t}{q_e} \tag{6}$$

Substitution of Eq. (6) in Eq. (5), the kinetic expression can be represented as

$$B_t = -0.4977 - \ln(1 - F) \tag{7}$$

As shown in Fig. 11, the plots are linear but do not pass through the origin. Moreover, the R^2 values of linear fitting under different initial dye concentration are in the range of 0.9660–0.9862 (Table 2), suggesting that film diffusion is the rate-controlling step in the adsorption process.

3.5. Adsorption isotherms

Isotherms study can describe how an adsorbate interacts with adsorbent. The isotherm provides a relationship between the concentration of dye in solution and the amount of dye adsorbed on the solid phase when both phases are in equilibrium. Fig. 12 shows the equilibrium isotherms for the adsorption of MB onto M-MWCNTs, and the equilibrium adsorption data were analyzed by using the Langmuir and Freundlich isotherm models [38,39]. The Langmuir isotherm is often applicable to a homogeneous adsorption surface with all the adsorption sites having equal adsorbate affinity, while the Freundlich isotherm is an empirical relation for adsorption over heterogeneous surfaces. The adsorption isotherm models of

Table 2
Intraparticle diffusion model parameters for the adsorption of MB onto the M-MWCNTs.

Intraparticle diffusion model							Boyd model	
C_0 (mg L^{-1})	$k_{i,1}$ (mg g^{-1} min$^{-1/2}$)	C_1 (mg g^{-1})	R^2	$k_{i,2}$ (mg g^{-1} min$^{-1/2}$)	C_2 (mg g^{-1})	R^2	Linear equation	R^2
10	1.65	11.03	0.8393	0.05	22.74	0.8573	$B_t = 0.03206t + 0.51055$	0.9660
20	2.72	20.07	0.9336	0.05	40.71	0.8755	$B_t = 0.0379t + 0.35216$	0.9862
30	2.43	25.91	0.9493	0.20	43.41	0.8662	$B_t = 0.02499t + 0.5966$	0.9831

Table 3
Comparison of the adsorption capacities of MB onto various adsorbents.

Adsorbents	Adsorption capacity ($mg\,g^{-1}$)	References
M-MWCNTs	48.06	This work
Rice husk	40.59	[40]
Fe(III)/Cr(III) hydroxide	22.8	[41]
clay	58.2	[42]
Carbonized citrus fruit peel	25.51	[43]
Silkworm exuviae	25.53	[44]
Diatomite	156.6	[45]
Tea waste	85.5	[46]
Iron terephthalate (MOF-235)	187	[47]

Langmuir and Freundlich can be represented in the nonlinear form as follows:

$$q_e = \frac{bq_m C_e}{1 + bC_e} \tag{8}$$

$$q_e = K_f C_e{}^{1/n} \tag{9}$$

where constant b is related to the energy of adsorption ($L\,mg^{-1}$), q_m is the Langmuir monolayer adsorption capacity ($mg\,g^{-1}$), K_f is roughly an indicator of the adsorption capacity, and $1/n$ is the adsorption intensity. The isotherms based on the experimental data and the parameters obtained from nonlinear regression by both models are shown in Fig. 12. The R^2 values of Langmuir and Freundlich models are 0.9873 and 0.8681, respectively, indicating that the Langmuir model is suitable for describing the adsorption equilibrium of MB onto M-MWCNTs. The monolayer adsorption capacity determined from the Langmuir isotherm is 48.06 $mg\,g^{-1}$. Table 3 compares the adsorption capacity of M-MWCNTs obtained in this study with different adsorbents previously used for removal of MB from aqueous solutions. The adsorption capacity of MB onto M-MWCNTs is higher than that of many other previously reported adsorbents [40–47], suggesting that the as-prepared M-MWCNTs have great potential application in dye removal from aqueous solution.

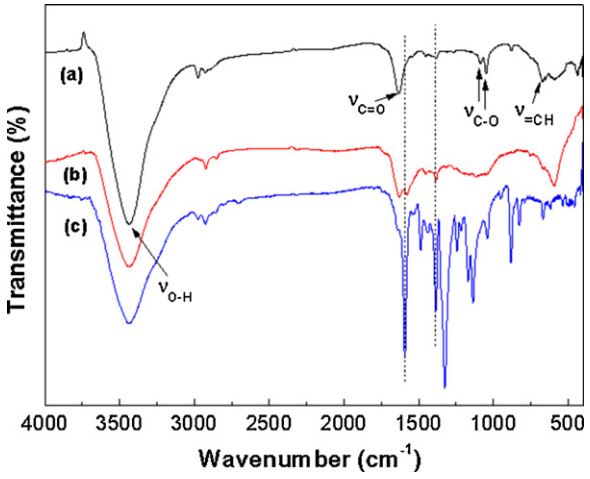

Fig. 13. FTIR spectra of M-MWCNTs before (a) and after (b) adsorption of the MB, and pure MB (c).

The essential characteristics of the Langmuir isotherm can be expressed in terms of a dimensionless constant separation factor R_L given by following relation that can be used to determine the feasibility of adsorption in a given concentration range over adsorbent [48].

$$R_L = \frac{1}{1 + bC_0} \tag{10}$$

The calculated R_L values at different initial dye concentration were in the range of 0.022–0.063, which lie between 0 and 1, confirming that the adsorption of dye over the adsorbent was favorable [49].

3.6. Adsorption mechanism

Fourier transform infrared (FTIR) spectroscopic analysis was performed to gain insight into the adsorption mechanism. Fig. 13

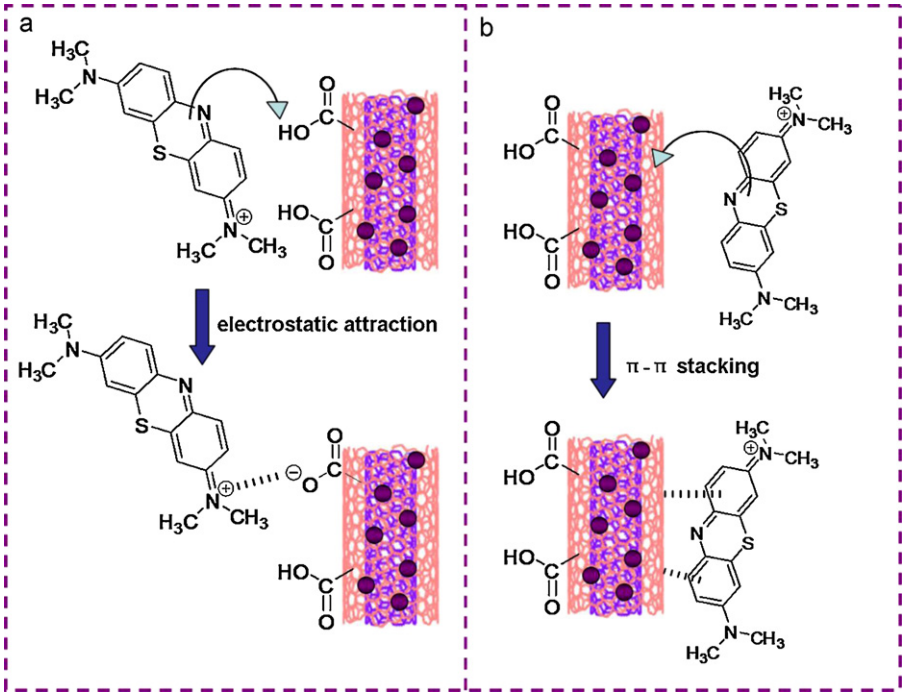

Fig. 14. Schematic illustration of the possible interaction between MWCNTs and MB: (a) electrostatic attraction and (b) π–π stacking.

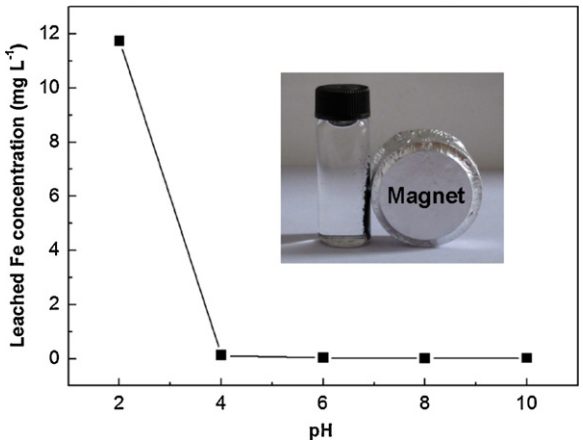

Fig. 15. Leached Fe content of M-MWCNTs under different pH levels.

shows the FTIR spectra of the M-MWCNTs before and after the MB adsorption. Based on the aforementioned results, the surface of M-MWCNTs has some oxygen-containing functional groups confirming by the presence of the characteristic absorption peaks at 3430 cm^{-1} (ν_{O-H}), 1574 cm^{-1} ($\nu_{C=O}$), 1385 cm^{-1} (δ_{O-H}), 1046 and 1092 cm^{-1} (ν_{C-O}). After adsorption of MB, the peak at 3430 cm^{-1} remains unchanged, which indicates that hydrogen bonding may not be an important process for MB adsorption onto the M-MWCNTs. However, the new absorption peak at 1600 cm^{-1} and the sharp peak at 1400 cm^{-1} can be clearly observed, which can be assigned to the vibration of the aromatic ring and C–N bond for MB [50]. This reflects the MB has been anchored on the surface of M-MWCNTs during the adsorption. It should be noted that the peaks associated with the ν_{C-O} and $\nu_{=CH}$ for the M-MWCNTs seem to be broadened and show a significant decrease in intensity. This can be explained by the following aspects: (i) MB is a kind of cationic dye which can be adsorbed easily by electrostatic forces on negatively charged surfaces. Therefore, the change in ν_{C-O} after adsorption may be ascribed to the electrostatic attraction between MWCNTs and MB; (ii) MB is also an ideally planar molecule and therefore can be easily adsorbed by MWCNTs by π–π stacking interactions between the aromatic backbone of the dye and hexagonal skeleton of MWCNTs, which may lead to the weakening the intensity of $\nu_{=CH}$ for the M-MWCNTs. The electrostatic attraction and π–π stacking interactions between MWCNTs and MB could be responsible for the adsorption ability of the M-MWCNTs, as schematically illustrated in Fig. 14.

3.7. Stability of adsorbent

Considering that leaching of metal ions from adsorbent into the treated water is undesirable, we further performed a leaching test in the aqueous solution at different pH levels to evaluate the stability of M-MWCNTs. Fig. 15 shows the concentrations of leached Fe under different pH levels. The leaching of Fe is negligible at pH over 4.0 and enhances significantly when pH is lower than 4.0. At pH 2.0, the concentration of the leached Fe ions is 11.74 mg L^{-1}. A similar trend was also previously observed for leaching of iron ions from Fe_3O_4-based composites [51–55]. Interestingly, M-MWCNTs after treated by strong acidic aqueous solution (pH 2.0) still possess perfect magnetic sensitivity under applied magnetic fields (inset in Fig. 15). These results imply that M-MWCNTs could maintain the good stability in various aqueous medium, which is advantageous for treating the weak acidic, neutral and basic wastewater.

4. Conclusions

In conclusion, magnetite-loaded multi-walled carbon nanotubes (M-MWCNTs) have been successfully synthesized by a facile one-pot solvothermal method. Adsorption ability of the M-MWCNTs is evaluated by choosing the methylene blue (MB) as an adsorbate. Batch adsorption tests demonstrate that the adsorption is affected by various conditions such as contact time, solution pH and initial dye concentration. Adsorption kinetics follows the pseudo-second-order model. The adsorption process is operated by both film diffusion and intraparticle diffusion, and the film diffusion is determined to be the rate-controlling step. Equilibrium data are fitted by Langmuir and Freundlich isotherms and the equilibrium data are better described by Langmuir isotherm model, with maximum monolayer adsorption capacity of 48.06 mg g^{-1}. The electrostatic attraction and π–π stacking interactions between MWCNTs and MB account for the high adsorptive performance of the M-MWCNTs. Interestingly, the resulting M-MWCNTs have a high magnetic sensitivity to the external magnetic field, thus providing an easy and efficient way for the separation of adsorbent from aqueous solution.

Acknowledgements

This work was supported by the National Natural Science Foundation of China (21103141), Open Project of Chemical Synthesis and Pollution Control Key Laboratory of Sichuan Province (11CSPC-(1-7)), Program for Scientific and Technological Innovative Team in Sichuan Provincial Universities (2010008) and Program for Scientific Research Innovation Team of China West Normal University.

References

[1] S.F. Li, Removal of crystal violet from aqueous solution by sorption into semi-interpenetrated networks hydrogels constituted of poly(acrylic acid-acrylamide-methacrylate) and amylose, Bioresour. Technol. 101 (2010) 2197–2202.
[2] N. Bao, Y. Li, Z.T. Wei, G.B. Yin, J.J. Niu, Adsorption of dyes on hierarchical mesoporous TiO_2 fibers and its enhanced photocatalytic properties, J. Phys. Chem. C 115 (2011) 5708–5719.
[3] M. Rafatullah, O. Sulaiman, R. Hashim, A. Ahmad, Adsorption of methylene blue on low-cost adsorbents: a review, J. Hazard. Mater. 177 (2010) 70–80.
[4] N. Daneshvar, M. Ayazloo, A.R. Khataee, M. Pourhassan, Biological decolorization of dye solution containing malachite green by microalgae *Cosmarium* sp, Bioresour. Technol. 98 (2007) 1176–1182.
[5] M. Riera-Torres, C. Gutiérrez-Bouzán, M. Crespi, Combination of coagulation–flocculation and nanofiltration techniques for dye removal and water reuse in textile effluents, Desalination 252 (2010) 53–59.
[6] T.-H. Kim, C. Park, J. Yang, S. Kim, Comparison of disperse and reactive dye removals by chemical coagulation and Fenton oxidation, J. Hazard. Mater. 112 (2004) 95–103.
[7] Y. He, G.M. Li, H. Wang, J.F. Zhao, H.X. Su, Q.Y. Huang, Effect of operating conditions on separation performance of reactive dye solution with membrane process, J. Membr. Sci. 321 (2008) 183–189.
[8] J. Labanda, J. Sabaté, J. Llorens, Experimental and modeling study of the adsorption of single and binary dye solutions with an ion-exchange membrane adsorber, Chem. Eng. J. 166 (2011) 536–543.
[9] A. Demirbas, Agricultural based activated carbons for the removal of dyes from aqueous solutions: a review, J. Hazard. Mater. 167 (2009) 1–9.
[10] W.-T. Tsai, K.-J. Hsien, H.-C. Hsu, Adsorption of organic compounds from aqueous solution onto the synthesized zeolite, J. Hazard. Mater. 166 (2009) 635–641.
[11] L.H. Ai, Y. Zhou, J. Jiang, Removal of methylene blue from aqueous solution by montmorillonite/$CoFe_2O_4$ composite with magnetic separation performance, Desalination 266 (2011) 72–77.
[12] L.H. Ai, J. Jiang, R. Zhang, Uniform polyaniline microspheres: a novel adsorbent for dye removal from aqueous solution, Synth. Met. 160 (2010) 762–767.
[13] X.M. Ren, C.L. Chen, M. Nagatsu, X.K. Wang, Carbon nanotubes as adsorbents in environmental pollution management: a review, Chem. Eng. J. 170 (2011) 395–410.
[14] D.D. Shao, J. Hu, C.L. Chen, G.D. Sheng, X.M. Ren, X.K. Wang, Polyaniline multiwalled carbon nanotube magnetic composite prepared by plasma-induced graft technique and its application for removal of aniline and phenol, J. Phys. Chem. C 114 (2010) 21524–21530.
[15] J. Hu, D.D. Shao, C.L. Chen, G.D. Sheng, J.X. Li, X.K. Wang, M. Nagatsu, Plasma-induced grafting of cyclodextrin onto multiwall carbon nanotube/iron

oxides for adsorbent application, J. Phys. Chem. B 114 (2010) 6779–6785.
[16] C.L. Chen, D.D. Shao, J.X. Li, X.K. Wang, Adsorption behavior of multiwall carbon nanotube/iron oxide magnetic composites for Ni(II) and Sr(II), J. Hazard. Mater. 164 (2009) 923–928.
[17] X.J. Peng, Z.K. Luan, Z.C. Di, Z.G. Zhang, C.L. Zhu, Carbon nanotubes-iron oxides magnetic composites as adsorbent for removal of Pb(II) and Cu(II) from water, Carbon 43 (2005) 855–894.
[18] J.L. Gong, B. Wang, G.M. Zeng, C.P. Yang, C.G. Niu, Q.Y. Niu, W.J. Zhou, Y. Liang, Removal of cationic dyes from aqueous solution using magnetic multi-wall carbon nanotube nanocomposite as adsorbent, J. Hazard. Mater. 164 (2009) 1517–1522.
[19] A.K. Mishra, S. Ramaprabhu, Magnetite decorated multiwalled carbon nanotube based supercapacitor for arsenic removal and desalination of seawater, J. Phys. Chem. C 114 (2010) 2583–2590.
[20] R.D. Waldron, Infrared spectra of ferrites, Phys. Rev. 99 (1955) 1727–1735.
[21] X.L. Tan, M. Fang, C.L. Chen, S.M. Yu, X.K. Wang, Counterion effects of nickel and sodium dodecylbenzene sulfonate adsorption to multiwalled carbon nanotubes in aqueous solution, Carbon 46 (2008) 1741–1750.
[22] X. Xie, L. Gao, J. Sun, Thermodynamic study on aniline adsorption on chemical modified multi-walled carbon nanotubes, Colloid Surf. A 308 (2007) 54–59.
[23] P.R. Chang, P.W. Zheng, B.X. Liu, D.P. Anderson, J.G. Yu, X.F. Ma, Characterization of magnetic soluble starch-functionalized carbon nanotubes and its application for the adsorption of the dyes, J. Hazard. Mater. 186 (2011) 2144–2150.
[24] B.P. Jia, L. Gao, Fabrication of tadpole-like magnetite/multiwalled carbon nanotube heterojunctions and their self-assembly under external magnetic field, J. Phys. Chem. B 111 (2007) 5337–5343.
[25] L.R. Kong, X.F. Lu, W.J. Zhang, Facile synthesis of multifunctional multiwalled carbon nanotubes/Fe_3O_4 nanoparticles/polyaniline composite nanotubes, J. Solid State Chem. 181 (2008) 628–636.
[26] H.Q. Cao, M.F. Zhu, Y.G. Li, J.H. Liu, Z. Ni, Z.Y. Qin, A highly coercive carbon nanotube coated with $Ni_{0.5}Zn_{0.5}Fe_2O_4$ nanocrystals synthesized by chemical precipitation-hydrothermal process, J. Solid State Chem. 180 (2007) 3218–3223.
[27] Y. Shan, L. Gao, Synthesis and characterization of phase controllable ZrO_2–carbon nanotube nanocomposites, Nanotechnology 16 (2005) 625–630.
[28] Y. Deng, C. Deng, D. Yang, C. Wang, S. Fu, X. Zhang, Preparation, characterization and application of magnetic silica nanoparticle functionalized multi-walled carbon nanotubes, Chem. Commun. 44 (2005) 5548–5550.
[29] T.-W. Lin, C.G. Salzmann, L.-D. Shao, C.-H. Yu, M.L.H. Green, S.-C. Tsang, Polyethylene glycol grafting and attachment of encapsulated magnetic iron oxide silica nanoparticles onto chlorosilanized single-wall carbon nanotubes, Carbon 47 (2009) 1415–1420.
[30] A.V. Korobeinyk, R.L.D. Whitby, J.J. Niu, Y. Gogotsi, S.V. Mikhalovsky, Rapid assembly of carbon nanotube-based magnetic composites, Mater. Chem. Phys. 128 (2011) 514–518.
[31] M. Sathishkumar, A.R. Binupriya, D. Kavitha, R. Selvakumar, R. Jayabalan, J.G. Choi, S.E. Yun, Adsorption potential of maize cob carbon for 2,4-dichlorophenol removal from aqueous solutions: equilibrium, kinetics and thermodynamics modeling, Chem. Eng. J. 147 (2009) 265–271.
[32] V.S. Mane, P.V.V. Babu, Studies on the adsorption of brilliant green dye from aqueous solution onto low-cost NaOH treated saw dust, Desalination 273 (2011) 321–329.
[33] S.F. Lim, Y.M. Zheng, S.W. Zou, Characterization of copper adsorption onto an alginate encapsulated magnetic sorbent by a combined FT-IR, XPS, and mathematical modeling study, Environ. Sci. Technol. 42 (2008) 2551–2556.
[34] S. Lagergren, About the theory of so-called adsorption of soluble substances, Kungliga Svenska Vetenskapsakademiens Handlingar 24 (1898) 1–39.
[35] Y.S. Ho, Adsorption of heavy metals from waste streams by peat, Ph.D. Thesis, University of Birmingham, Birmingham, 1995.
[36] W.J. Weber Jr., J.C. Morris, Kinetics of adsorption on carbon from solution, J. Sanit. Eng. Div. Am. Soc. Civ. Eng. 89 (1963) 31–60.
[37] G.E. Boyd, A.W. Adamson, L.S. Meyers, The exchange adsorption of ions from aqueous solutions by organic zeolites. II: kinetics, J. Am. Chem. Soc. 69 (1947) 2836–2848.
[38] I. Langmuir, The constitution and fundamental properties of solids and liquids, J. Am. Chem. Soc. 38 (1916) 2221–2295.
[39] H.M.F. Freundlich, Over the adsorption in solution, Z. Phys. Chem. 57 (1906) 385–471.
[40] V. Vadivelan, K. Kumar, Equilibrium, kinetics, mechanism, and process design for the sorption of methylene blue onto rice husk, J. Colloid Interface Sci. 286 (2005) 90–100.
[41] C. Namasivayam, S. Sumithra, Removal of direct red 12B and methylene blue from water by adsorption onto Fe(III)/Cr(III) hydroxide, an industrial solid waste, J. Environ. Manage. 74 (2005) 207–215.
[42] A. Gurses, C. Dogar, M. Yalcin, M. Acikyildiz, R. Bayrak, S. Karaca, The adsorption kinetics of the cationic dye, methylene blue, onto clay, J. Hazard. Mater. B131 (2006) 217–228.
[43] S. Dutta, A. Bhattacharyya, A. Ganguly, S. Gupta, S. Basu, Application of response surface methodology for preparation of low-cost adsorbent from citrus fruit peel and for removal of methylene blue, Desalination 275 (2011) 26–36.
[44] H. Chen, J. Zhao, G.L. Dai, Silkworm exuviae—a new non-conventional and low-cost adsorbent for removal of methylene blue from aqueous solutions, J. Hazard. Mater. 186 (2011) 1320–1327.
[45] M.A. Al-Ghouti, M.A.M. Khraisheh, S.J. Allen, M.N. Ahmad, The removal of dyes from textile wastewater: a study of the physical characteristics and adsorption mechanisms of diatomaceous earth, J. Environ. Manage. 69 (2003) 229–238.
[46] M.T. Uddin, M.A. Islam, S. Mahmud, M. Rukanuzzaman, Adsorptive removal of methylene blue by tea waste, J. Hazard. Mater. 164 (2009) 53–60.
[47] E. Haque, J.W. Jun, S.H. Jhung, Adsorptive removal of methyl orange and methylene blue from aqueous solution with a metal-organic framework material, iron terephthalate (MOF-235), J. Hazard. Mater. 185 (2011) 507–511.
[48] T.W. Weber, R.K. Chakravorti, Pore and solid diffusion models for fixed-bed adsorbers, AIChE J. 20 (1974) 228–238.
[49] G. McKay, Adsorption of dyestuffs from aqueous solution with activated carbon. I. Equilibrium and batch contact time studies, J. Chem. Technol. Biotechnol. 32 (1982) 759–772.
[50] L. Xiong, Y. Yang, J.X. Mai, W.L. Sun, C.Y. Zhang, D.P. Wei, Q. Chen, J.R. Ni, Adsorption behavior of methylene blue onto titanate nanotubes, Chem. Eng. J. 156 (2010) 313–320.
[51] B.S. Inbaraj, B.H. Chen, Dye adsorption characteristics of magnetite nanoparticles coated with a biopolymer poly(γ-glutamic acid), Bioresour. Technol. 102 (2011) 8868–8876.
[52] J.H. Wang, S.R. Zheng, Y. Shao, J.L. Liu, Z.Y. Xu, D.Q. Zhu, Amino-functionalized Fe_3O_4@SiO_2 core–shell magnetic nanomaterial as a novel adsorbent for aqueous heavy metals removal, J. Colloid Interface Sci. 349 (2010) 293–299.
[53] J.-F. Liu, Z.-S. Zhao, G.-B. Jiang, Coating Fe_3O_4 magnetic nanoparticles with humic acid for high efficient removal of heavy metals in water, Environ. Sci. Technol. 42 (2008) 6949–6954.
[54] C.H. Yang, J.J. Du, Q. Peng, R.R. Qiao, W. Chen, C.L. Xu, Z.G. Shuai, M.Y. Gao, Polyaniline/Fe_3O_4 nanoparticle composite: synthesis and reaction mechanism, J. Phys. Chem. B 113 (2009) 5052–5058.
[55] M.H. Do, N.H. Phan, T.D. Nguyen, T.T.S. Pham, V.K. Nguyen, T.T.T. Vu, T.K.P. Nguyen, Activated carbon/Fe_3O_4 nanoparticle composite: fabrication, methyl orange removal and regeneration by hydrogen peroxide, Chemosphere (2011), doi:10.1016/j.chemosphere.2011.1007.1023.